JOURNAL OF MATERIALS SCIENCE 37 (2002) 3915–3923

Processing and characterization of carbon nanotube/poly(styrene-co-butyl acrylate) nanocomposites

A. DUFRESNE*, M. PAILLET, J. L. PUTAUX
CERMAV-CNRS, Université Joseph Fourier-BP 53, 38041 Grenoble cedex 9, France
E-mail: Alain.Dufresne@cermav.cnrs.fr

R. CANET, F. CARMONA, P. DELHAES
CRPP-CNRS, Avenue Albert Schweitzer, 33600 Pessac, France
E-mail: delhaes@crpp.u-bordeaux.fr

S. CUI
Department of Chemistry, Tianjin University, Tianjin 300072, People's Republic of China

Nanocomposite materials were prepared from an amorphous poly(styrene-co-butyl acrylate) latex as the matrix using an aqueous suspension of carbon nanotubes as the filler. After stirring, the preparations were cast and evaporated. The morphology of the resulting films was examined by scanning electron microscopy and a good dispersion of the filler was observed, except for the 5 wt% filled sample. The electrical conductivity and mechanical behavior in both the linear and non-linear ranges were analyzed. From conductivity measurements, a clear percolation threshold has been observed for a relatively low critical volume fraction around 1.5%. The mechanical characterization displayed a continuous reinforcing effect of the carbon nanotubes without lowering of the elongation at break up to 3 wt%. The thermal stability of the composites was strongly improved by carbon nanotubes loading. For instance, the terminal zone was shifted by 115 K with only 15 wt% of nanotubes.

1. Introduction

There is currently a considerable interest in processing polymeric composite materials filled with nanosized rigid particles (essentially inorganic but also organic). This class of material is called "nanocomposites". This growing interest originates from both the point of view of fundamental properties determination and the development of new applications. Indeed, because the building blocks of a nanocomposite are nanoscale, they have an enormous interface area, and therefore there are a lot of interfaces between the two intermixed phases compared to usual composites. The interfacial specific area can be in the order of a few 100 cm^2 per gram of material and the effect of interfacial phenomena are assumed to be noticeable on the volumic properties. In addition, the mean distance between particles is all the smaller since their size is small, favoring filler-filler interactions. Finally, the improvement of the properties of the material is often achieved without strong lowering of properties such as impact strength or ability to plastic deformation.

Nanofillers applications and therefore growth of new nanocomposites can be yet restricted owing on the one hand to their availability and on the other hand to the strong tendency of nanoparticles to aggregate, preventing a high level of dispersion within the polymer matrix, which is the key parameter required for high mechanical properties [1].

Because of their outstanding properties, carbon nanotubes have numerous potential applications [2]. Ajayan [1] wrote a review article on the structure and properties of carbon nanotubes, single wall as well as multiwall forms. The latter can be considered as cylindrical whiskers constructed from ideal in-plane graphite architecture and it is interesting to prepare nanocomposites from them. One class of nanotube materials is nanotube-polymer composites in which the nanotube architecture is established within a host matrix material. The nanotubes should confer high conductivity at lower loadings than carbon black or micrometer-sized fillers, such as carbon fibers or stainless steel fibers. In addition, theoretical calculations and experimental measurements on individual carbon nanotubes have shown that these one dimensional materials have exceptional mechanical properties compared to carbon fibers. The elastic modulus of the single wall carbon nanotubes is estimated in the range to be around 1 TPa [3–5].

However, the effective utilization of nanotubes in composite applications strongly depends on the ability to disperse the nanotubes homogeneously throughout

*Author to whom all correspondence should be addressed.

the matrix without destroying the integrity of the nanotubes. Furthermore, good interfacial bonding is required to achieve load transfer across the filler-matrix interface, a necessary condition for improving the mechanical properties of composites. Fabrication and investigation of polymer-nanotube composites present considerable challenges and have been the topic of several recent studies which used epoxy resins [6–11] and thermoplastic polymers [12–14] as the matrix material.

In the present work, stable carbon nanotubes aqueous suspensions were prepared and used as a reinforcing phase in a thermoplastic matrix. By analogy with previous works performed at CERMAV and which deal with cellulose or starch microcrystals reinforced nanocomposite systems [15–24], composite materials were processed using an aqueous suspension of polymer, i.e., a latex, as the matrix.

2. Experimental

2.1. Multiwalled carbon nanotubes preparation

The carbon nanotubes were prepared as described elsewhere [25]. The nickel catalyst was reduced around 500°C and then the growth of carbon nanotubes from nickel catalyzed pyrolysis of CH_4 was carried out at 600°C in a mixture of CH_4-H_2 (9 : 1). The reaction was quenched with Ar. A classical method of purification was used to desorb the graphitic surface. These multiwall nanotubes with mean diameter around 30–50 nm were first heat-treated under vacuum at 100°C for 7 h and then kept under vacuum at room temperature for 14 h.

2.2. Carbon nanotubes aqueous suspensions

As already described [26] the purified carbon nanotubes were suspended in a distilled water solution of 1 wt% sodium dodecyl sulfate (SDS) surfactant. Sonication was used to break up and suspend the nanotube bulks. The sonication step was performed 5 times for 2 min with 20×10^{-6} m^3 suspension volumes with a freezing step between each 2 min sonication. A stable 0.3 wt% carbon nanotubes suspension resulted. This suspension was concentrated by centrifugation (14,000 rpm for 1 h) and the residue was sonicated again 4 times for 2 min. A stable 1.85 wt% carbon nanotubes aqueous suspension resulted.

2.3. Film Processing

A latex obtained by the copolymerization of styrene (34 wt%) and butyl acrylate (64 wt%), and containing 1 wt% acrylic acid and 1 wt% acrylamide was used as the matrix. The aqueous polymer suspension contained spherical particles with an average diameter around 150 nm and had a 30 wt% solid fraction. The glass-rubber transition temperature (T_g) of the copolymer is around 0°C. The carbon nanotubes dispersion was mixed with the suspension of latex in order to obtain composite films with a weight fraction of nanotubes ranging from 0 to 15 wt%. After stirring, the preparations were cast in a Teflon mold and films were obtained by storing the casting at 35°C to allow both water evaporation and polymer particle coalescence. The evaporation time was around 15 days and 0.8 mm thick films resulted.

2.4. Electron microscopy

Drops of the dilute nanotube suspension were deposited onto glow-discharged carbon-coated TEM grids and allowed to dry. The samples were observed at room temperature using a Philips CM200 electron microscope operated at 80 kV for conventional observation and 200 kV for high-resolution imaging. The micrographs were recorded on Agfa Scientia films.

Scanning electron microscopy (SEM) was performed to investigate the morphology of the nanocomposite films with a JEOL JSM-6100 instrument. The specimens were frozen under liquid nitrogen, then fractured, mounted, coated with gold/palladium on a JEOL JFC-1100E ion sputter coater, and observed. SEM micrographs were obtained using 7 kV secondary electrons.

2.5. Dynamic mechanical analysis (linear range)

Dynamic mechanical tests were accomplished using a Rheometrics RSA2 spectrometer in the tensile mode. Test conditions were chosen in such a way that the measurements were in the linear viscoelasticity region (the maximum strain ε was around 10^{-4}). The specimen was a thin rectangular strip ($30 \times 5 \times 0.8$ mm). The setup measured the complex tensile modulus E^*, i.e., the storage component E' and the loss component E'', as well as the ratio of the two components, i.e., $\tan\delta (= E''/E')$. In the present work, results are displayed through E' and $\tan\delta$. Measurements were performed in isochronal conditions at 1 Hz, and the temperature was varied by steps of 3 K between 200 and 450 K.

2.6. Tensile tests (non linear range)

The nonlinear mechanical behavior of the carbon nanotubes-based composites was analyzed using an Instron 4301 testing machine in tensile mode, with a load cell of 100 N capacity. The specimen was a thin rectangular strip ($\sim 30 \times 5 \times 0.8$ mm) and the gap between pneumatic jaws at the start of each test was adjusted to 20 mm.

The stress-strain curves were obtained at room temperature at a strain rate $d\varepsilon/dt = 3.33 \times 10^{-2}$ s^{-1} (crosshead speed = 20 mm.min^{-1}). The true strain ε can be determined by $\varepsilon = \ln(L/L_0)$, where L and L_0 are the length during the test, and the length at zero time, respectively. The true stress σ was calculated by $\sigma = F/S$, where F is the applied load and S is the cross-sectional area. S was determined assuming that the total volume of the sample remained constant, so that $S = S_0 \times L_0/L$, where S_0 is the initial cross-sectional area. This assumption is fully valid in our case since the samples display an elastomeric behavior at room temperature. Owing to the high strains involved for rubbery polymers during tensile tests, it is preferable to use true stress and strain in order to account for the actual stress and strain conditions. Stress versus strain curves were plotted and the tensile or Young's modulus (E) was measured from the slope of the low strain region in the vicinity of $\sigma = \varepsilon = 0$ ($[d\sigma/d\varepsilon]_{\varepsilon \to 0}$).

Ultimate mechanical properties were also characterized. Ultimate elongation was characterized by the true strain at break, $\varepsilon_b = \ln[1 + (\Delta L_b/L_0)]$, where ΔL_b is the elongation at break. The nominal strain at break can be expressed as $\varepsilon_n = \Delta L_b/L_0$. Three to four replicates of the composites were measured in order to ensure reproducibility of measurement and mechanical tensile data were averaged.

2.7. Electrical conductivity measurements

The room temperature electrical conductivity has been measured using a standard four points configuration (except for the most insulated compounds for which an electrometer has been used) in two orthogonal directions along the main directions.

3. Results and discussion

3.1. Nanotube morphology

TEM micrographs of the dilute suspension dried on a carbon film show aggregates of tortuous vermicular objects with a width ranging between 50 and 80 nm and a length of several micrometers (Fig. 1a). Sometimes, one can see that both ends of individual nanotubes are different (Fig. 1b).

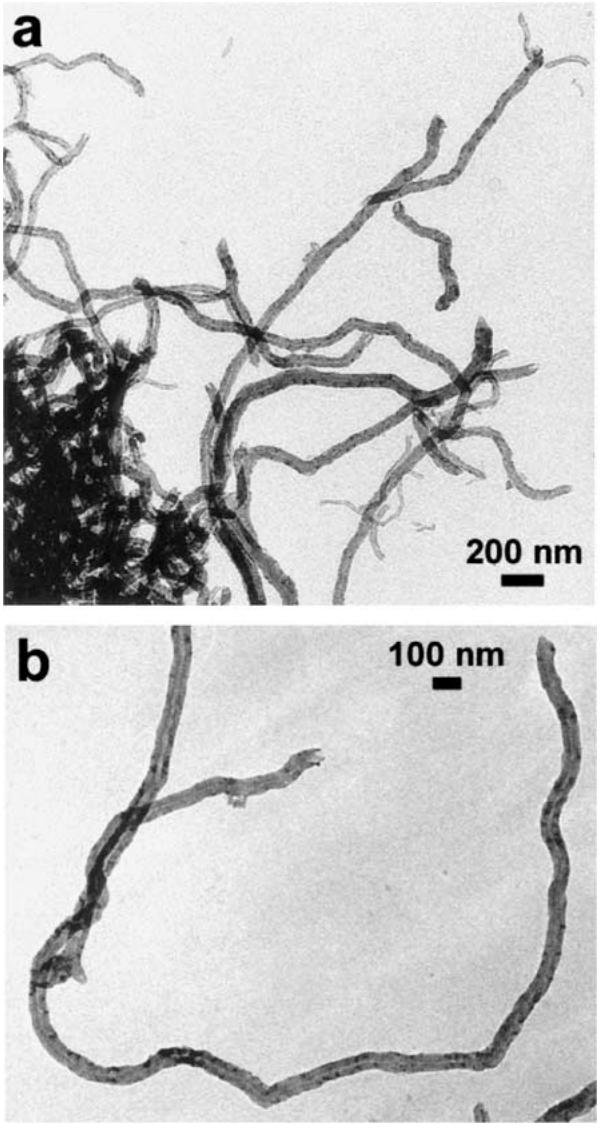

Figure 1 Bright field TEM micrographs of carbon nanotubes. (a) Typical aggregate of nanotubes. (b) Individual tube whose ends appear to be different.

High resolution images allow to visualize the arrangement of aromatic atomic planes separated by 0.34 nm. The nanotubes exhibit a peculiar structure. They are multiwalled but the graphitic planes are not parallel to the tube axis. Depending on the tube, they form an angle of 15 or 30° with the tube axis (Fig. 2). Such a structure has been observed by Hamwi *et al*. [27] and described by Audier *et al*. [28]. It is also similar to the structure of boron nitride filaments prepared by catalytic methods [29]. One end of the tube is closed with a conical shape (Fig. 2a) while the other end opens out (Fig. 2b). Thus, it appears that the nanotubes are formed by a long pile of graphitic cones, as schematized in Fig. 2d. Looking carefully at the central part of the tube, one can see 'bridges' formed by groups of curved planes forming the caps of the cones (Fig. 2c). Consequently, although the nanotubes are hollow in the center, the cavity is not continuous. In addition, considering that the latex cannot penetrate inside the nanotube, the central cavity will remain empty, a fact that might have to be taken into account in the properties of the composite materials.

The peculiar structure of the nanotubes has to be taken into account when examining both the nature of the surface from the nanotube in contact with the polymer matrix and the mechanical properties of the nanotubes. In a nanotube made of cylindrical parallel planes, the surface is a graphitic plane. In our case, the tube is described as a pile of cones so the surface correspond to the borders of the aromatic planes (Fig. 2) where most of the active sites are present.

3.2. Morphological characterization of nanocomposite films

To evaluate the morphology of the carbon nanotubes/poly(S-co-BuA) materials, examination of the surface of fractured films was carried out using SEM. Fig. 3 shows low magnification SEM observations of the nanocomposite films, just after fracture, filled with different nanotube contents. The freshly fractured surface of unfilled poly(S-co-BuA) film (Fig. 3a) is smooth. As the nanotube content increases up to 3 (Fig. 3b) and 5 wt% (Fig. 3c), the fractured surface is rougher owing to the presence of the filler within the polymeric matrix. At this scale of observation, carbon nanotubes could appear to be homogeneously dispersed in the matrix for low filler content (3 wt%—Fig. 3b), whereas nanotubes aggregates appear as clusters (indicated by arrows) for the 5 wt% filled sample (Fig. 3c). This clustering phenomenon was also observed for higher carbon contents (not shown) but the occurrence of the clusters was lower with respect to the loading level. It is clear from Fig. 3c that the nanotubes are heterogeneously dispersed within the polymeric matrix for the 5 wt% filled sample. Carbon nanotubes aggregate and form filler domains surrounded by the poly(S-co-BuA) matrix. It is also worth noting that these nanotube-rich regions occur irregularly in the sample and especially in the film thickness. This gradient of nanotubes concentration and clustering effect is most likely induced

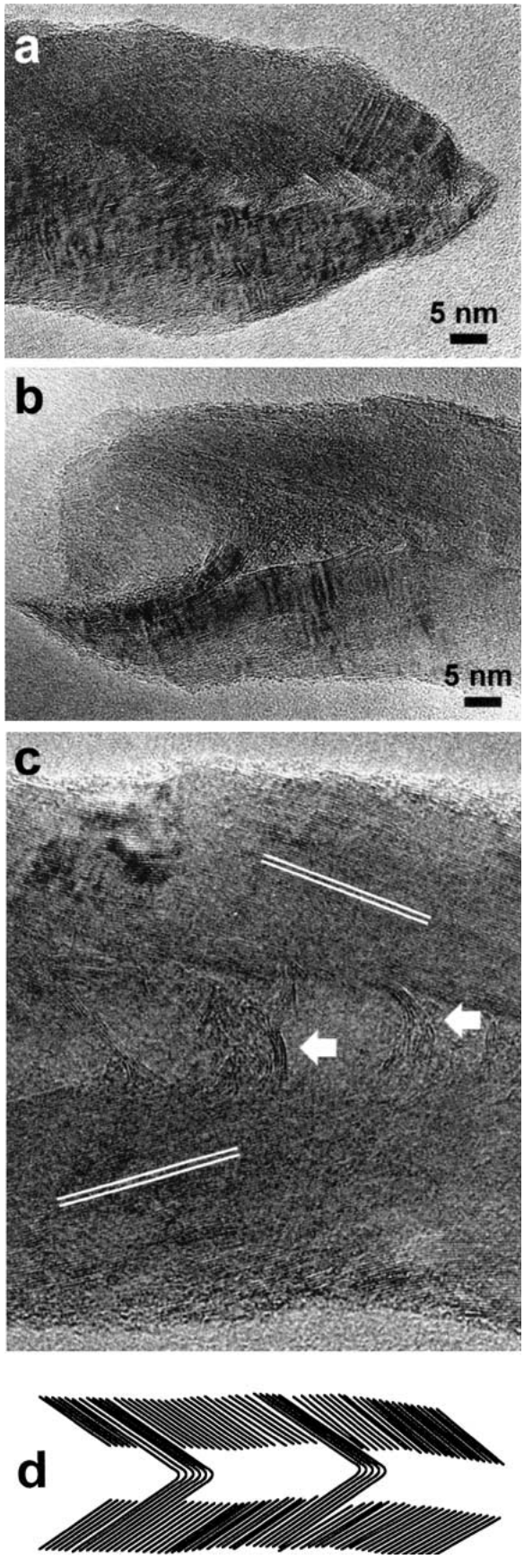

Figure 2 High resolution TEM micrographs of nanotubes. The lattice fringes correspond to graphitic planes separated by 0.34 nm. The planes form a 30° angle with respect to the tube axis. (a) Closed conical end. (b) Opened out end. (c) Central part of the tube. One can see the hollow cavity with bridges formed by groups of caps of graphitic cones. (d) Schematic projection of the distribution of aromatic planes in a carbon nanotube. The tube is formed by a pile of graphitic cones with open or closed caps. The caps of the closed cones form bridges that break the continuity of the central hollow cavity.

by the casting-evaporation processing technique. For highly filled samples (5 wt% and up), the evaporation step most probably induces translational motion of the nanotubes leading to their sedimentation.

Fig. 4 shows high magnification SEM observations of the freshly fractured surface of nanocomposite films, filled with different nanotube contents up to 7 wt%. Nanotubes appear like homogeneously dispersed raised domains. The ridges in Fig. 4 are most likely to be due to the fracture behavior of the polymer.

3.3. Electrical conductivity of nanocomposite films

The plot of the electrical resistivity versus the carbon loading expressed in weight% is presented in Fig. 5 for two orthogonal directions. These results show clearly that a percolation threshold is occurring below 3 wt%, i.e., corresponding to a critical volume fraction around 1.5% taking $\approx$2000 kg/m^3 for the density of multiwall carbon nanotubes [14]. This critical volume fraction value is around twice lower than the approximate value already published in the literature using the polyvinyl alcohol as a matrix [30].

For comparison with the usual composites using carbon fibers, two remarks have to be made. This very low critical volume fraction is in agreement with the value already found for short fibers randomly distributed in a polymer [31]. This is characteristic of a very anisotropic shape or aggregate formation for the conducting charge. For example in structured carbon blacks exhibiting local organization a similar low critical volume fraction has been also found [32, 33]. It is also well known that the percolation threshold is sensitive to the polymer type in carbon particles-filled polymers [34]. This effect is due to the role of interfacial properties as also found for these nanocomposites where the interfacial role is enhanced. Indeed, these results (Fig. 5) show that more detailed studies are necessary to describe this critical behavior.

3.4. Dynamic mechanical analysis (linear range)

Dynamic mechanical analysis measurements were performed on pure poly(S-co-BuA) matrix and up to 15 wt% carbon nanotubes composites. Fig. 6 shows a plot of log (E'/Pa) (Fig. 6a) and tan δ (Fig. 6b) at 1 Hz as a function of temperature for the various nanotubes compositions. The unfilled poly(S-co-BuA) matrix displays typical behavior of amorphous thermoplastic polymer. At low temperature the copolymer is in the glassy state and the modulus slightly decreases with increase in temperature but remains roughly constant (around 1 GPa). Then, a rapid decrease in the elastic tensile modulus, by more than 3 decades, is observed corresponding to the glass-rubber transition. This modulus drop is therefore ascribed to an energy dissipation phenomenon involving cooperative motions of long chain sequences. It is displayed in Fig. 6b in the concomitant relaxation process where the mechanical loss factor tan δ passes through a maximum around 285 K.

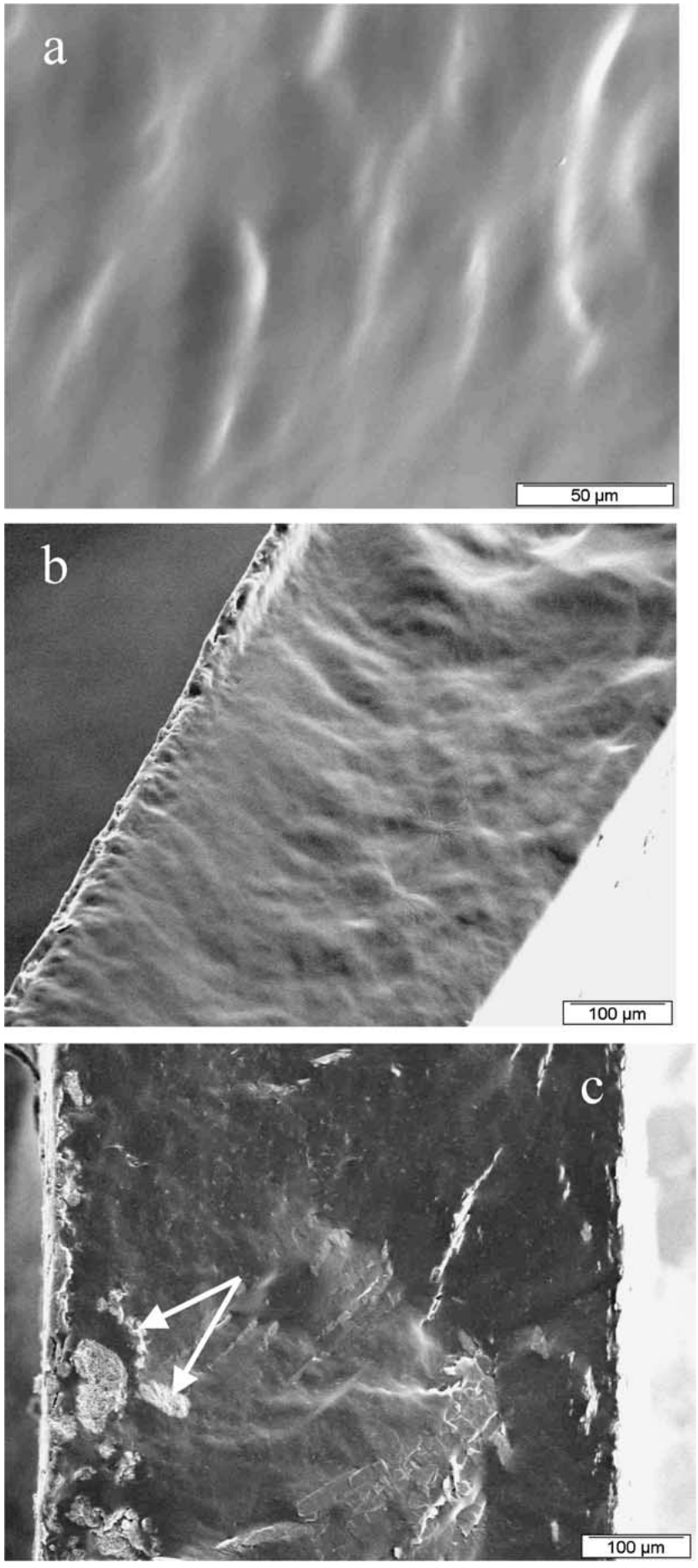

Figure 3 Low magnification scanning electron micrographs from the fractured surface of (a) unfilled poly(S-co-BuA) matrix (×500) and related composites (×160) filled with (b) 3 wt% and (c) 5 wt% of carbon nanotubes.

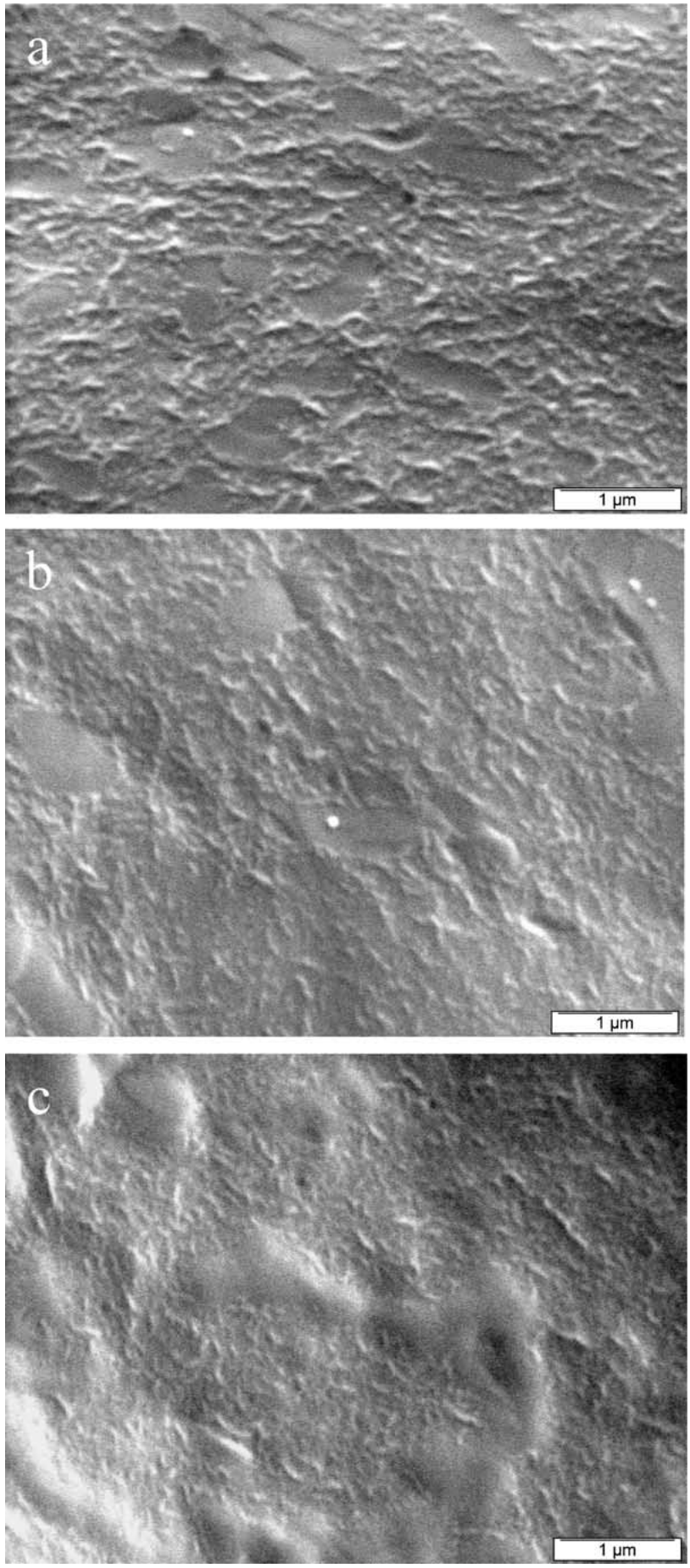

Figure 4 High magnification scanning electron micrographs from the fractured surface of (a) 2 wt%, (b) 3 wt%, and (c) 7 wt% of carbon nanotubes.

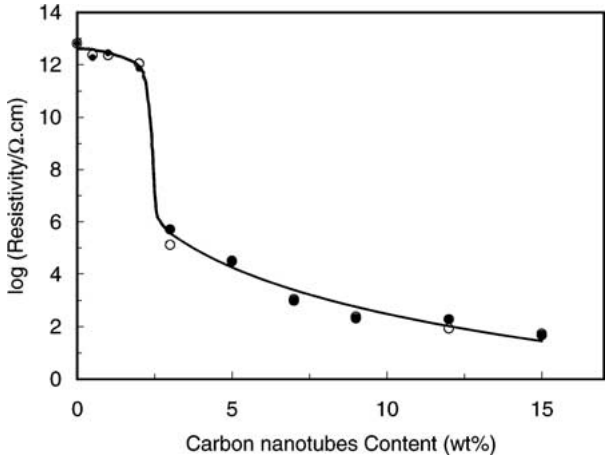

Figure 5 Electrical resistivity at room temperature of carbon nanotubes/poly(S-co-BuA) nanocomposites measured in the parallel (●) and orthogonal (○) directions versus nanotubes content (the solid line serves to guide the eye).

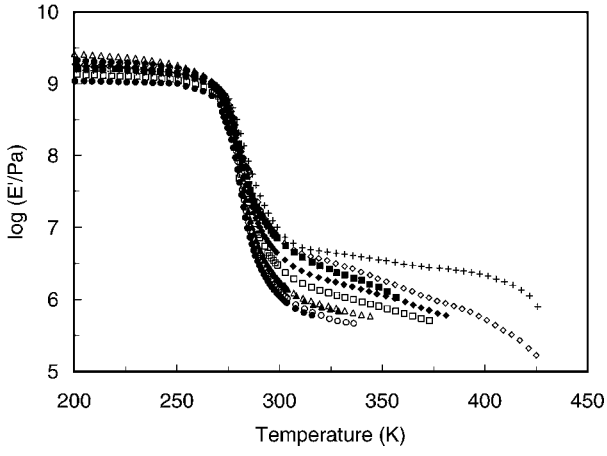

(a)

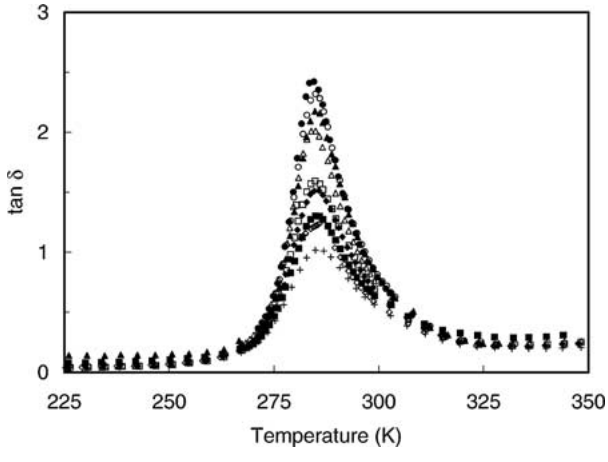

(b)

Figure 6 (a) Logarithm of the storage tensile modulus E' and (b) loss angle tangent tan δ, vs temperature at 1 Hz for carbon nanotubes/poly (S-co-BuA) nanocomposites filled with 0 (●), 1 (○), 2 (▲), 3 (△), 5 (■), 7 (□), 9 (◆), 12 (◇), and 15 wt% (+) of carbon nanotubes.

The temperature position of this relaxation process is known to depend on the frequency of the measurement. The rubbery modulus of the polymer remains roughly constant (around 1 MPa), up to the terminal zone, for which the elastic tensile modulus becomes lower with temperature and the experimental setup fails to measure it.

The films that contain carbon nanotubes have a slight increase in their storage modulus below T_g (Fig. 6a). The composite modulus increases up to about 3 GPa for the highly filled material. However, the exact determination of the glassy modulus depends on the precise knowledge of the sample dimensions. In this case, at room temperature, the composite films were soft and it was difficult to obtain a constant and precise thickness along these samples. In order to minimize this effect, the samples were frozen in liquid nitrogen prior to any experiment to accurately measure their dimensions. In addition, in this temperature range, the difference between the elastic modulus of the carbon nanotubes and that of the matrix is not high enough to easily appreciate a reinforcement effect with only few percents of nanotubes.

Above T_g and for highly filled materials, a greater increase in the composite modulus is observed with increasing weight fraction of carbon nanotubes. For instance, the relaxed modulus at $T_g + 50°C$ (∼320 K) of a film containing 15 wt% nanotubes is 10 times higher than that of the matrix. However, this reinforcing effect is very low compared to what was observed for poly(S-co-BuA) reinforced with cellulose whiskers [15–17, 19]. For these nanocomposite systems, the great reinforcing effect was assigned to specific interactions between whiskers and the formation of a rigid percolating cellulose network within the thermoplastic matrix. It appears that such mechanical percolation phenomenon is not observed for the poly(S-co-BuA) filled with carbon nanotubes. It is worth noting that cellulose whiskers are stiff and straight well-defined objects. In contrast nanotubes remain twisted and curved when processed to make polymer composites, and the advantage of high aspect ratio may not be realized because of their highly deformable behavior.

In addition to this reinforcing effect at high temperature, carbon nanotubes improve the thermal stability of the composite materials. Indeed, whereas the stiffness of the non-reinforced matrix decreases with temperature, the relaxed modulus of composites remains roughly constant up to a temperature which value increases with the filler content. For instance, the modulus of a film containing 15 wt% of nanotubes drops at 430 K, whereas the terminal zone occurs at 315 K for the unfilled material. This phenomenon can be most probably ascribed to good interfacial bonding between the filler and the matrix, which prevents irreversible flow of the matrix macromolecular chains at high temperature. It is most likely due to the atomistic surface of nanotubes exhibiting active sites at their surface (Fig. 2).

It is also worth noting the peculiar behavior of the 5 wt% filled material. The rubbery modulus of this composite sets between the one of the 9 and 12 wt% filled sample, respectively. This peculiarity can be most probably related to the SEM observations and could be ascribed to the strong occurrence of nanotube clusters within the matrix with respect to the global loading level for this composition. Assuming the irregular occurrence of nanotube-rich regions in the film thickness, this material can be represented as a multilayered composite composed of the superimposition of high

and low modulus layers. The formation of stiff parallel nanotube-rich layers is assumed to govern the macroscopic mechanical behavior of the composite.

Fig. 6b shows that no shift of the main relaxation process is observed. This relaxation process involves cooperative motions of long chain sequences associated with the anelastic manifestation of the glass-rubber transition of poly(S-co-BuA). The magnitude of this relaxation process, which is related to the magnitude of the modulus drop, depends upon both the number of mobile entities and their contribution to the compliance. It decreases as the carbon nanotubes loading increases. This means a decrease of the mobile units at T_g. This result may be explained by the decrease of matrix material amount, responsible for damping properties. However, the relative damping is not related simply to the filler volume fraction but also to interfacial effects due to changes in the properties of the polymer by adsorption onto the filler particle [24]. These interfacial phenomena are expected to be important owing to the high specific area of carbon nanotubes.

3.5. Tensile tests (non-linear range)

The non-linear tensile mechanical behavior of both the unfilled poly(S-co-BuA) matrix and related carbon nanotubes filled composites was analyzed at room temperature, in order to evaluate the effect of the filler loading on the high strain properties. True stress vs. true strain curves for pure poly(S-co-BuA) matrix and up to 15 wt% carbon nanotubes composites at 25°C are reported in Fig. 7. For each measurement, it was observed that the strain was macroscopically homogeneous and uniform along the sample, until its break. The lack of any necking phenomenon confirms the homogeneous nature of these composites at the scale of a few hundred nm^3.

The unfilled matrix exhibits an elastic non-linear behavior typical of amorphous polymer at $T > T_g$. The stress continuously increases with the strain. The copolymer is in the rubbery state and its elasticity from entropic origin is ascribed to the presence of numerous entanglements due to high molecular weight chains. The stronger hardening observed for true strains higher than 2 results from the stretching of macromolecular chains in the tensile direction.

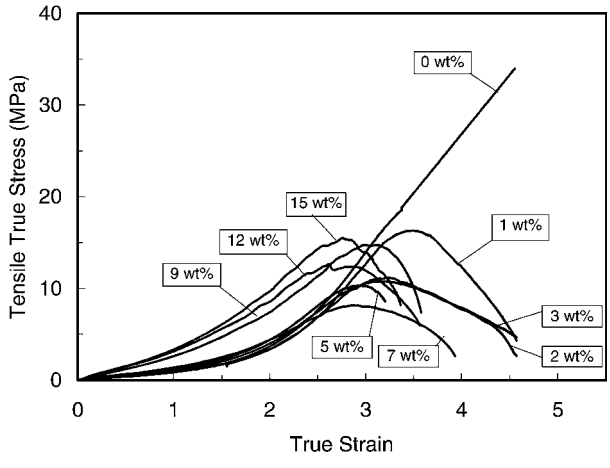

Figure 7 True stress versus true strain curves of carbon nanotubes/poly(S-co-BuA) nanocomposites at 25°C, $d\varepsilon/dt = 3.33 \times 10^{-2}\,s^{-1}$. The carbon nanotubes contents are indicated in the figure.

TABLE I Mechanical properties of carbon nanotubes/poly(S-co-BuA) nanocomposites : tensile modulus, E, true ultimate strain, ε_b, and nominal ultimate strain, ε_n

Carbon nanotubes content (wt%)	E (MPa)	ε_b (%)	ε_n (%)
0	0.52	4.56	95
1	0.865	4.56	95
2	0.83	4.56	95
3	0.99	4.56	95
5	1.88	3.22	24
7	1.00	3.83	45
9	2.06	3.50	32
12	3.00	3.40	29
15	3.54	3.33	27

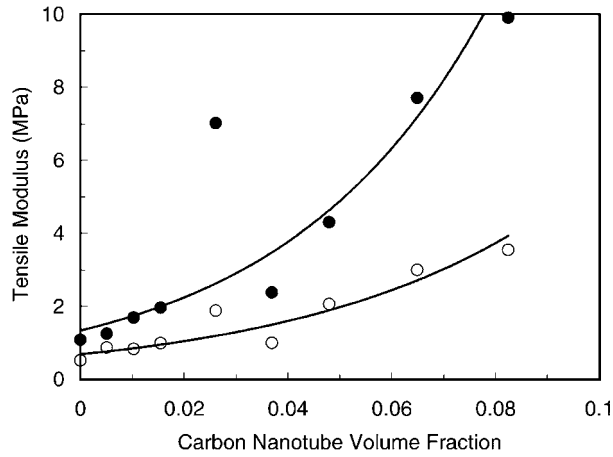

Figure 8 Tensile modulus of carbon nanotubes/poly(S-co-BuA) nanocomposites measured at room temperature from dynamic mechanical analysis (●) and tensile tests (○) versus nanotubes content (the solid lines serve to guide the eye).

With increasing carbon nanotubes content, the behavior of the material progressively changes from an elastomeric behavior to a plastic or pseudo plastic behavior for which the stress increases, passes through a maximum and then decreases with increasing strain. The presence of the carbon nanotubes results in an increase of both the tensile or Young's modulus as determined from the slope of the stress vs. strain curves in the vicinity of $\sigma = \varepsilon = 0$, as already observed from dynamic mechanical analysis, and the stress for a given strain. Results are plotted in Fig. 8, as well as the relaxed storage modulus measured at 300 K from dynamic mechanical analysis, vs. nanotubes content. Experimental data are also collected in Table I. It is worth noting that the glass–rubber transition temperature is close to the room temperature and therefore the modulus value is strongly sensitive to any temperature fluctuation. The tensile moduli are in agreement, but systematically lower, with storage tensile modulus values measured at room temperature (Fig. 6a). It is well known that the tensile modulus greatly depends on the experimental conditions, such as strain rate and temperature.

It is observed that the presence of carbon nanotubes weakens the composites at high loading level (higher than 3 wt%) since the elongation at break decreases

with nanotubes content. In addition, the loading of the matrix results in a damage of the polymer because the stretching of the macromolecular chains of the copolymer under high strain induces a lower and even non-existent hardening phenomenon compared to the unfilled matrix. Thus for true strains higher than 3 the unfilled matrix displays the higher tensile strength.

For these high strain experiments again, a peculiar behavior is reported for the 5 wt% filled sample. The tensile modulus is higher than for the 7 wt% filled sample and the elongation at break is surprisingly the lowest one for all the tested compositions. It is well known that particle aggregation tends to reduce the strength of a material even though the agglomeration may be strong enough to increase the initial modulus [35]. Agglomerates are weak points in the material and break fairly easily when a stress is applied to them. Broken agglomerate then behaves as a strong stress concentrator. In addition, since agglomerates are larger than the primary filler particles, they produce weaker materials than composites containing the dispersed particles.

4. Conclusions

A soft method has been used with success to produce polymer nanocomposites with multiwall carbon nanotubes. The choice of multiwall rather than single wall nanotubes was to try to reinforce the matrix without any intrinsic deformation as observed (buckling or polygonization effect for example). A good interfacial interaction, related to the hydrophobic surface of graphite, has been observed. As a resulting effect a clear percolation threshold has been observed for a quite low value ($\phi_C \sim 1.5\%$) with a good load transfer to the matrix. The thermal stability of the composites was also strongly improved by carbon nanotubes loading. Associated with their characteristics as electromagnetic radiation shielding they can be useful as protective conducting layers.

Acknowledgment

The authors would like to thank Mrs. Danièle Dupeyre (CERMAV) for the SEM observations.

References

1. P. M. AJAYAN, *Chem. Rev.* **99** (1999) 1787.
2. B. I. YAKOBSON and R. E. SMALLEY, *Am. Sci.* **85** (1997) 324.
3. M. M. TREACY, T. W. EBBESEN and J. M. GIBSON, *Nature (London)* **381** (1996) 678.
4. E. W. WONG, P. E. SHEEHAN and C. M. LIEBER, *Science* **277** (1997) 1971.
5. J. P. SALVETAT, G. A. BRIGGS, J. M. BONARD, R. R. BACSA, A. J. KULIK, T. STOCKLI, N. A. BURNHAY and L. FURRO, *Phys. Rev. Lett.* **81** (1999) 944.
6. P. M. AJAYAN, O. STEPHAN, C. COLLIEX and D. TRAUTH, *Science* **265** (1994) 1212.
7. H. D. WAGNER, O. LOURIE, Y. FELDMAN and R. TENNE, *Appl. Phys. Lett.* **72** (1998) 188.
8. O. LOURIE and H. D. WAGNER, *ibid.* **73** (1998) 3527.
9. L. S. SCHADLER, S. C. GIANNARIS and P. M. AJAYAN, *ibid.* **73** (1998) 3842.
10. O. LOURIE, D. M. COX and H. D. WAGNER, *Phys. Rev. Lett.* **81** (1998) 1638.
11. J. SANDLER, M. S. P. SHAFFER, T. PRASSE, W. BAUHOFER, K. SCHULTE and A. H. WINDLE, *Polymer* **40** (1999) 5967.
12. L. JIN, C. BOWER and O. ZHOU, *Appl. Phys. Lett.* **73** (1998) 1197.
13. C. BOWER, R. ROSEN, L. JIN, J. HAN and O. ZHOU, *ibid.* **74** (1999) 3317.
14. D. QIAN, E. C. DICKEY, R. ANDREWS and T. RANTELL, *ibid.* **76** (2000) 2868.
15. V. FAVIER, G. R. CANOVA, J. Y. CAVAILLÉ, H. CHANZY, A. DUFRESNE and C. GAUTHIER, *Polym. Adv. Techn.* **6** (1995) 351.
16. V. FAVIER, J. Y. CAVAILLÉ and H. CHANZY, *Macromolecules* **28** (1995) 6365.
17. W. HELBERT, J. Y. CAVAILLÉ and A. DUFRESNE, *Polym. Compos.* **17** (1996) 604.
18. A. DUFRESNE, J. Y. CAVAILLE and W. HELBERT, *Macromolecules* **29** (1996) 7624.
19. *Idem.*, *Polym. Compos.* **18** (1997) 198.
20. A. DUFRESNE and J. Y. CAVAILLE, *J. Polym. Sci. Part B: Polym. Phys.* **36** (1998) 2211.
21. L. CHAZEAU, M. PAILLET and J. Y. CAVAILLÉ, *ibid.* **37** (1999) 2151.
22. D. DUBIEF, E. SAMAIN and A. DUFRESNE, *Macromolecules* **32** (1999) 5765.
23. A. DUFRESNE, M. B. KELLERHALS and B. WITHOLT, *ibid.* **32** (1999) 7396.
24. A. DUFRESNE, *Compos. Interfaces* **7** (2000) 53.
25. S. CUI, C. Z. LU, Y. L. QIAD and L. CUI, *Carbon* **37** (1999) 2070.
26. B. VIGOLO, A. PENICAUD, C. COULON, C. SAUDER, R. PAILLER, C. JOURNET, P. BERNIER and P. POULIN, *Science* **290** (2000) 1331.
27. A. HAMWI, H. ALVERGNAT, S. BONNAMY and F. BEGUIN, *Carbon* **35** (1997) 723.
28. P. GLEIZE, M. C. SHOULER, P. GADELLE and M. CAILLET, *J. Mater. Sci.* **29** (1994) 1575.
29. M. AUDIER, A. OBERLIN, M. OBERLIN, M. COULON and L. BONNETAIN, *Carbon* **19** (1981) 217.
30. M. S. P. SHAFFER and A. H. WINDLE, *Adv. Mater.* **11** (1999) 937.
31. F. CARMONA, F. BARREAU, P. DELHAES and R. CANET, *J. de Physique Lettres* **41** (1980) 531.
32. M. A. J. MICHELS, J. C. M. BROKKEN-ZIJP, W. M. GROENEWOUD and A. KNOESTER, *Physica* A **157** (1989) 529.
33. L. J. ADRIAANSE, J. A. REEDIJK, P. A. A. TEUNISSEN, H. B. BROM, M. A. J. MICHELS and J. C. M. BROKKEN-ZIJP, *Phys. Rev. Lett.* **78** (1997) 1755.
34. K. MIYASAKA, K. WATANABE, E. JOJIMA, H. AIDA and M. SUMITA, *J. Mater. Sci.* **17** (1982) 1610.
35. L. E. NIELSEN, in "Mechanical Properties of Polymers and Composites," Vol. 2 (Marcel Dekker, New York, 1974).

Received 21 August 2001
and accepted 11 April 2002